into the simulation (representing possible impurities from a catalyst) instead of carbon adatoms gives a considerable deviation from the experimental profiles, which supports again the notion that the defect structure involves only carbon adatoms and vacancies. The more frequent defect structure of an adatom–vacancy pair is shown schematically in Fig. 4e.

Defects in a graphene layer, such as topological defects, vacancies and adatoms, have been experimentally proved to be numerous and stable under electron irradiation. We can envisage more diversified applications in nanocarbon materials by taking advantage of these defects, which can be induced locally during electron irradiation. Combining the present experiments with the scanning probe microscopy technique and its associated electron transport measurements[27,28] is of particular interest and might allow us to obtain more comprehensive information on the physical and chemical properties of defective carbon nanostructures. □

## Methods

### Electron microscopy

A Schottky-type field emission gun (JEOL, JEM-2010F) was used for HR-TEM. We employed optimized parameters for imaging, well fitted to a high-efficiency charge-coupled device (CCD)-based camera (Gatan model 794) with a fibre-optic coupling to the YAG scintillators. To enhance phase contrast and decrease thermally induced drift in the specimen as much as possible, a multi-exposure procedure was employed so that we could decrease the exposure time to 1 s and sum a few images with specimen-drift corrections to limit electron irradiation damage and the consequent thermally induced structural changes, high-speed blanking was used to prevent exposure of the specimen to the electron beam during each readout by the CCD detector. A typical electron dose was ~60,000 electrons $nm^{-2}$ for a HR-TEM image. To realize both sufficient sensitivity and sufficient resolution to visualize the single graphene layer, we used a lower accelerating voltage (120 keV) for the incident electron beam close to the displacement threshold, for the following three reasons: first, to double the scattering cross-section of carbon atoms being observed; second, so that carbon adatoms were not blasted away from the graphene layers and could therefore be observed (note that the threshold for electron irradiation on carbon materials is taken to be 80–140 keV; and last, to optimize the efficiency of the CCD detector for image acquisition. As indicated by the red graph in Supplementary Fig. S1 (bottom inset), we carefully chose the experimental conditions as a compromise with the moderate accelerating voltage of the incident electron beam so that the CTF could have a local maximum at 0.21–0.23 nm, which corresponds exactly to the repeat distance of the zig-zag chain of a graphene layer (Supplementary Fig. S1, top inset). The confidence level for the detection of a single carbon atom exceeds 80%. All the experiments shown here were performed at room temperature because raising the temperature might have led to an instantaneous relaxation of these atomic defects.

### Chiral index determination

The apparent chiral angle ($\alpha$) can be measured to an accuracy of ~3°; measurement of the diameter ($d$) in the HR-TEM image might involve about 10% error, as previously quoted in refs 15 and 29. We made a systematic study with a series of image simulations for the nanotubes of various diameters (Supplementary Fig. S3). Taking all of the microscope parameters into account, the true diameter can be therefore deduced from the apparent tube diameter to within the 3% error. The inclination of the specimen to the incident electron beam cannot be neglected in this experiment. We selected the tubes to examine which were as parallel as possible to the observed plane within a few degrees of inclination. Optical diffraction is strongly influenced by the inclination of the sample, whereas conventional electron diffraction is weakly dependent on it. The distortion and disappearance of symmetrical hexagons in optical diffraction is able to assist in the estimation of inclination angles. Our simulation tells us that the chiral angle can be measured to an accuracy of ~3° when the inclination angle is within 10°.

Received 13 February; accepted 6 July 2004; doi:10.1038/nature02817.


1. Hansson, A., Paulsson, M. & Stafström, S. Effect of bending and vacancies on the conductance of carbon nanotubes. *Phys. Rev. B* **62,** 7639–7644 (2000).
2. Ewels, C. P., Heggie, M. I. & Briddon, P. R. Adatoms and nanoengineering of carbon. *Chem. Phys. Lett.* **351,** 178–182 (2002).
3. Nordlund, K., Keinonen, J. & Mattila, T. Formation of ion irradiation induced small-scale defects on graphite surfaces. *Phys. Rev. Lett.* **77,** 699–702 (1996).
4. Krasheninnikov, A. V., Nordlund, K., Sirviö, M., Salonen, E. & Keinonen, J. Formation of ion-irradiation-induced atomic-scale defects on walls of carbon nanotubes. *Phys. Rev. B* **63,** 245405 (2001).
5. Kelly, K. F. & Halas, N. J. Determination of α and β site defects on graphite using $C_{60}$-adsorbed STM tips. *Surf. Sci.* **416,** L1085–L1089 (1998).
6. Ouyang, M., Huang, J.-L., Cheung, C. L. & Lieber, C. M. Atomically resolved single-walled carbon nanotube intramolecular junctions. *Science* **291,** 97–100 (2001).
7. Meyer, R. R. *et al.* A composite method for the determination of the chirality of single walled carbon nanotube. *J. Microsc.* **212,** 152–157 (2003).
8. Zuo, J. M., Vartanyants, I., Gao, M., Zhang, R. & Nagahara, L. A. Atomic resolution imaging of a carbon nanotube from diffraction intensities. *Science* **300,** 1419–1421 (2003).
9. Stone, A. J. & Wales, D. J. Theoretical studies of icosahedral $C_{60}$ and some related species. *Chem. Phys. Lett.* **128,** 501–503 (1986).
10. Telling, R. H., Ewels, C. P., El-Barbary, A. A. & Heggie, M. I. Wigner defects bridge the graphite gap. *Nature Mater.* **2,** 333–337 (2003).
11. El-Barbary, A. A., Telling, R. H., Ewels, C. P., Heggie, M. I. & Briddon, P. R. Structure and energetics of the vacancy in graphite. *Phys. Rev. B* **68,** 144107 (2003).
12. Krasheninnikov, A. V. *et al.* Adsorption and migration of carbon adatoms on carbon nanotubes: Density-functional *ab initio* and tight-binding studies. *Phys. Rev. B* **69,** 073402 (2004).
13. Ewels, C. P., Telling, R. H., El-Barbary, A. A., Heggie, M. I. & Briddon, P. R. Metastable Frenkel pair defect in graphite: Source of Wigner energy? *Phys. Rev. Lett.* **91,** 25505 (2003).
14. Lehtinen, P. O. *et al.* Magnetic properties and diffusion of adatoms on a graphene sheet. *Phys. Rev. Lett.* **91,** 17202 (2003).
15. Kociak, M., Hirahara, K., Suenaga, K. & Iijima, S. How accurate can the determination of chiral indices of carbon nanotubes be? *Eur. Phys. J. B* **32,** 457–469 (2003).
16. Ajayan, P. M., Ravikumar, V. & Charlier, J.-C. Surface reconstructions and dimensional changes in single-walled carbon nanotubes. *Phys. Rev. Lett.* **81,** 1437–1440 (1998).
17. Smith, B. W. & Luzzi, D. E. Electron irradiation effects in single wall carbon nanotubes. *J. Appl. Phys.* **90,** 3509–3515 (2001).
18. Iijima, S. *et al.* Nano-aggregates of single-walled graphitic carbon nano-horns. *Chem. Phys. Lett.* **309,** 165–170 (1999).
19. Yakobson, B. I., Samsonidze, G. & Samsonidze, G. G. Atomistic theory of mechanical relaxation in fullerene nanotubes. *Carbon* **38,** 1675–1680 (2000).
20. Banhart, F. Irradiation effects in carbon nanostructures. *Rep. Prog. Phys.* **62,** 1181–1221 (1999).
21. Hahn, J. R., Kang, H., Song, S. & Jeon, I. C. Observation of charge enhancement induced by graphite atomic vacancy: A comparative STM and AFM study. *Phys. Rev. B* **53,** R1725–R1728 (1996).
22. Orlikowski, D., Buongiorno Nardelli, M., Bernholc, J. & Roland, C. Theoretical STM signatures and transport properties of native defects in carbon nanotubes. *Phys. Rev. B* **61,** 14194–14203 (2000).
23. Asari, E., Kitajima, M., Nakamura, K. G. & Kawabe, T. Thermal relaxation of ion-irradiation damage in graphite. *Phys. Rev. B* **47,** 11143–11148 (1993).
24. Hjort, M. & Stafström, S. Modeling vacancies in graphite via the Hückel method. *Phys. Rev. B* **61,** 14089–14094 (2000).
25. Krasheninnikov, A. V., Nordlund, K. & Keinonen, J. Production of defects in supported carbon nanotubes under ion irradiation. *Phys. Rev. B* **65,** 165423 (2002).
26. Lu, A. J. & Pan, B. C. Nature of single vacancy in achiral carbon nanotubes. *Phys. Rev. Lett.* **92,** 105504 (2004).
27. Wildöer, J. W. G., Venema, L. C., Rinzler, A. G., Smalley, R. E. & Dekker, C. Electronic structure of atomically resolved carbon nanotubes. *Nature* **391,** 59–62 (1998).
28. Odom, T. W., Huang, J.-L., Kim, P. & Lieber, C. M. Atomic structure and electronic properties of single-walled carbon nanotubes. *Nature* **391,** 62–64 (1998).
29. Kociak, M. *et al.* Linking chiral indices and transport properties of double-walled carbon nanotubes. *Phys. Rev. Lett.* **81,** 155501 (2002).


**Supplementary Information** accompanies the paper on **www.nature.com/nature**.

**Acknowledgements** We thank M. Kociak for his instructions on the chiral index determination of SWNTs; C. Ewels and Y. Miyamoto for discussions on defective carbon structures; and M. Yudasaka and S. Bandow for help with specimen preparation. Work on HR-TEM is supported by the NEDO Nano-Carbon Technology project. A.H. was supported by Research Fellowships of the Japan Society for the Promotion of Science for Young Scientists.

**Competing interests statement** The authors declare that they have no competing financial interests.

**Correspondence** and requests for materials should be addressed to K.S. (suenaga-kazu@aist.go.jp).

# Chemical remodelling of cell surfaces in living animals

**Jennifer A. Prescher[1]*, Danielle H. Dube[1]* & Carolyn R. Bertozzi[1,2]**

[1]*Department of Chemistry, University of California, Berkeley, California 94720, USA*
[2]*Department of Molecular and Cell Biology and Howard Hughes Medical Institute, University of California, Materials Sciences Division, Lawrence Berkeley National Laboratory, Berkeley, California 94720, USA*

* These authors contributed equally to this work

**Cell surfaces are endowed with biological functionality designed to mediate extracellular communication. The cell-surface repertoire can be expanded to include abiotic functionality through the biosynthetic introduction of unnatural sugars into cellular glycans, a process termed metabolic oligosaccharide engineering[1,2]. This technique has been exploited in fundamental studies of glycan-dependent cell–cell and virus–cell interactions[3–5] and**

**also provides an avenue for the chemical remodelling of living cells[6–8]. Unique chemical functional groups can be delivered to cell-surface glycans by metabolism of the corresponding unnatural precursor sugars. These functional groups can then undergo covalent reaction with exogenous agents bearing complementary functionality. The exquisite chemical selectivity required of this process is supplied by the Staudinger ligation of azides and phosphines, a reaction that has been performed on cultured cells without detriment to their physiology[7,9]. Here we demonstrate that the Staudinger ligation can be executed in living animals, enabling the chemical modification of cells within their native environment. The ability to tag cell-surface glycans *in vivo* may enable therapeutic targeting and non-invasive imaging of changes in glycosylation during disease progression.**

Central to the process of chemical cell-surface remodelling is the concept of bio-orthogonality. The pair of functional groups chosen for the cell-surface transformation must be mutually reactive under physiological conditions and, at the same time, remain inert to the biological environment. We previously developed a reaction that meets these criteria—the Staudinger ligation between azides and a specific class of phosphines (Fig. 1a)[7]. The azide is essentially unreactive with biological nucleophiles yet readily condenses with exogenously delivered phosphine reagents. If the phosphine is functionalized as shown in Fig. 1a, its reaction with azides forms a stable amide bond with concomitant release of nitrogen and methanol and conversion to the phosphine oxide.

Azides can be metabolically introduced into cell-surface glycans by virtue of the unnatural substrate tolerance of certain carbohydrate biosynthetic pathways. For example, the unnatural sugar *N*-α-azidoacetylmannosamine (ManNAz) is metabolized by cultured cells to *N*-α-azidoacetyl sialic acid (SiaNAz) and incorporated into membrane glycoconjugates (Fig. 1b)[7,9]. Azido analogues of *N*-acetylgalactosamine and *N*-acetylglucosamine can be similarly incorporated into cellular glycoproteins[10,11]. Once displayed on the cell surface, the azides are poised for Staudinger ligation with phosphine compounds to generate unique cell-surface epitopes. In addition, chemical tagging of azide-labelled glycans permits the identification of specific glycoprotein subtypes from the proteome[10,11]. Beyond its utility in elaborating glycan structures, the Staudinger ligation has been used in numerous biological applications[12,13].

So far, the unique features of the Staudinger ligation have only been exploited in biochemical or cell-based systems. There are obvious advantages, however, to applying this reaction in the physiologically authentic environment of a living organism—especially in the context of metabolic oligosaccharide engineering. Cellular glycosylation patterns could be probed within organs, and cells could be remodelled to change their immunogenic properties in a temporally controlled fashion. Moreover, the ability to chemically alter cell surfaces in a targeted manner is applicable to the diagnosis and treatment of human diseases associated with aberrant glycosylation[14–16]. To realize this vision would require that azido-sugar metabolism and the Staudinger ligation both proceed in living animals.

Here we report that cells can be chemically modified in laboratory mice by metabolism of peracetylated ManNAz ($Ac_4$ManNAz) and subsequent Staudinger ligation. We chose the sialic acid biosynthetic pathway as a vehicle for the display of cell-surface azides based on the efficient conversion of $Ac_4$ManNAz to SiaNAz observed in previous cell culture studies[7]. Furthermore, it has been reported that analogues of the natural substrate *N*-acetylmannosamine (ManNAc) with extended *N*-acyl chains are converted to the corresponding sialic acids in rats, suggesting that these precursors can access organs *in vivo*[8]. In cell culture, $Ac_4$ManNAz is a more efficient substrate for SiaNAz biosynthesis than free ManNAz owing to its facile entry into cells by passive diffusion[17]. The acetyl groups are then removed by carboxyesterases within the cell. Similar esterases exist at high levels in rodent serum[18,19], the activity of which might reduce the concentration of biologically available $Ac_4$ManNAz. Thus, we first investigated the conversion of $Ac_4$ManNAz to SiaNAz in the plasma esterase-deficient mouse strain $Es1^e/Es1^e$ (refs 18, 20).

$Es1^e/Es1^e$ mice were administered daily doses of $Ac_4$ManNAz (0–300 mg $kg^{-1}$) intraperitoneally for 7 days. On the eighth day, the mice were euthanized and their splenocytes (cells rich in sialosides) were isolated. The presence of cell-surface azides was quantified by Staudinger ligation *ex vivo* with a phosphine probe comprising a Flag peptide (Phos–Flag) (shown schematically in Fig. 1c)[21]. Treatment with a fluorescein isothiocyanate-labelled anti-Flag antibody

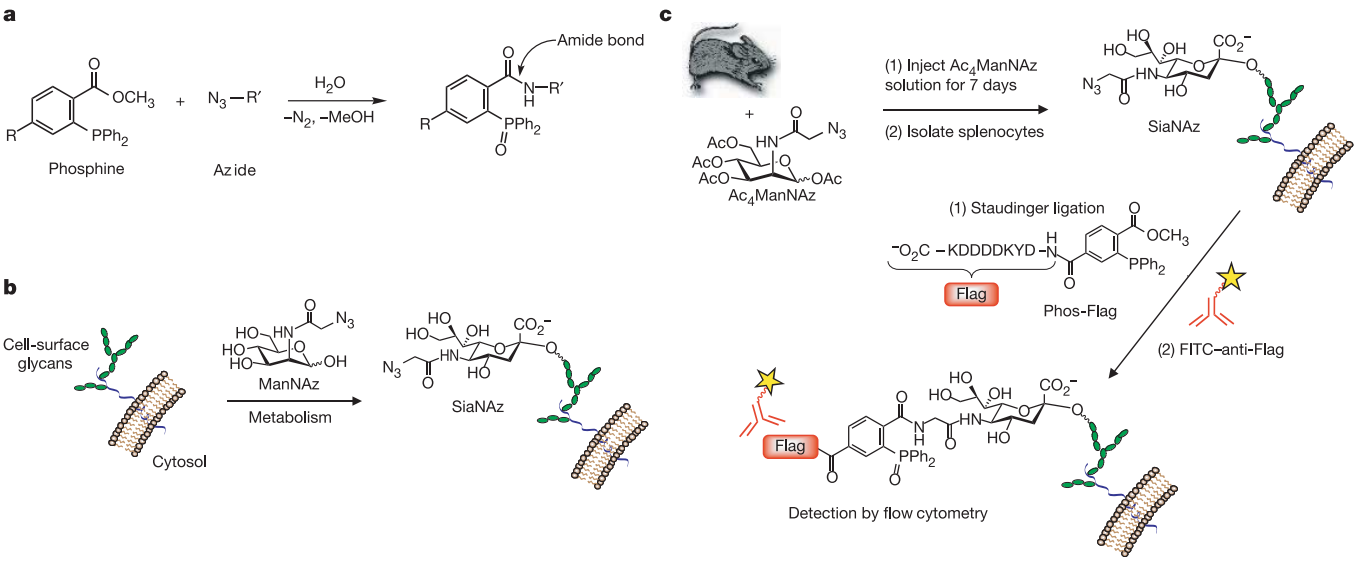


**Figure 1** The Staudinger ligation and metabolic oligosaccharide engineering. **a**, The Staudinger ligation of an azide and functionalized phosphine results in the formation of an amide bond. **b**, Azides can be delivered to cell-surface glycoconjugates by metabolism of ManNAz to SiaNAz. **c**, Experimental overview for investigating the metabolic conversion of $Ac_4$ManNAz *in vivo*. Splenocytes from mice treated with the azido sugar were collected and probed for the presence of cell-surface azides using Phos–Flag. Labelled cells were treated with FITC–anti-Flag and analysed by flow cytometry.

(FITC–anti-Flag) and subsequent flow cytometry analysis produced the data depicted in Fig. 2a, b. Splenocytes from mice treated with $Ac_4$ManNAz exhibited a dose-dependent increase in fluorescence, which was significantly higher than the signal observed with splenocytes from vehicle-treated mice. These data suggest that $Ac_4$ManNAz is metabolized to SiaNAz in murine splenocytes. Notably, treatment with the highest dose of $Ac_4$ManNAz produced no apparent adverse physiological effects over 7 days, as determined by monitoring feeding habits, weight and overall activity.

To assess the importance of peracetylation for the biological availability of ManNAz, we treated mice with $Ac_4$ManNAz or an equimolar amount of the free sugar. No azides were observed on splenocytes from mice treated with free ManNAz as assessed by flow cytometry, whereas $Ac_4$ManNAz produced a robust azide-dependent signal (Fig. 2c). Acetyl protection therefore considerably increases the efficiency of azido-sugar metabolism *in vivo*. Surprisingly, the extent of metabolic labelling in murine splenocytes was found to be identical in the plasma esterase-deficient $Es1^e/Es1^e$ and wild-type B6D2F1 mice treated with $Ac_4$ManNAz (Fig. 2d). This finding suggests that a broad variety of experimental mouse models are amenable to chemical cell-surface remodelling.

We probed further for the presence of azido sugars in glycoproteins from a panel of murine organs. Selected organs were collected from mice that had been administered daily doses of $Ac_4$ManNAz (300 mg $kg^{-1}$) or vehicle for 7 days. These organs were homogenized, and the soluble fractions were reacted with Phos–Flag and analysed by western blot. As shown in Fig. 3a, labelled glycoproteins were only observed in organ lysates from mice exposed to $Ac_4$ManNAz. Discrete bands were observed from heart, kidney and liver lysates, but not from brain or thymus homogenates. The liver is known to secrete numerous sialylated glycoproteins and is a target of first-pass metabolism, factors that may explain the robust labelling observed in that organ. Notably, the kidney and heart lack significant levels of UDP-GlcNAc 2-epimerase[22], the enzyme that produces endogenous ManNAc. Low levels of endogenous ManNAc might provide ManNAz with a competitive advantage for metabolic labelling in these organs. Glycoprotein expression levels and tissue access might also contribute to the observed distribution of azides.

To confirm that SiaNAz is indeed the host of glycoprotein-associated azides, we incubated splenocytes from $Ac_4$ManNAz-treated and untreated mice with sialidase and evaluated the effects on cell-surface azide levels by Staudinger ligation with Phos–Flag. As shown in Fig. 3b, sialidase treatment significantly reduced the cell-surface fluorescence. Similarly, sialidase treatment of serum glycoproteins from mice administered $Ac_4$ManNAz reduced Phos–Flag labelling in a dose-dependent manner (Fig. 3c). Finally, direct characterization of SiaNAz was accomplished by sialic acid analysis of heart tissue lysates from $Ac_4$ManNAz-treated mice with com-

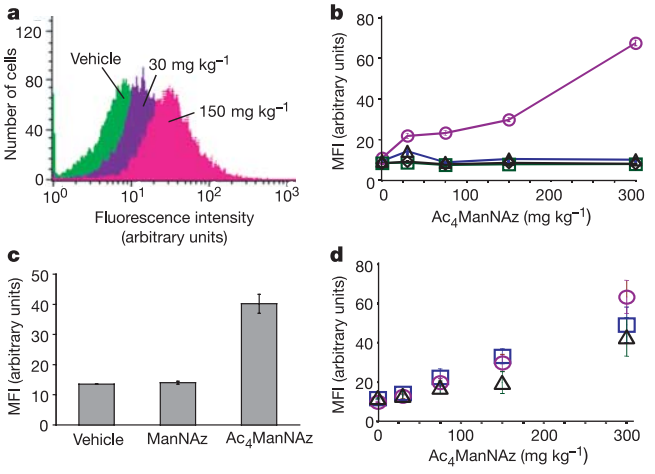


**Figure 2** $Ac_4$ManNAz is metabolized *in vivo*. **a**, Flow cytometry analysis of splenocytes from $Ac_4$ManNAz-treated mice. **b**, Mean fluorescence intensity (MFI) of the cells from **a** as a function of azido-sugar dose (circles). Assay controls included unlabelled splenocytes from $Ac_4$ManNAz-treated mice (squares), splenocytes from $Ac_4$ManNAz-treated mice incubated with Phos–Flag followed by a class-matched control monoclonal antibody (diamonds), and splenocytes from $Ac_4$ManNAz-treated mice incubated with FITC–anti-Flag only (triangles). **c**, MFI of splenocytes from $Ac_4$ManNAz- and ManNAz-treated $Es1^e/Es1^e$ mice. **d**, MFI of splenocytes from $Es1^e/Es1^e$ mice (triangles) or wild-type B6D2F1 mice (circles, males; squares, females) treated with $Ac_4$ManNAz. Error bars represent the standard deviation of the mean for three replicate Staudinger ligation reactions. For **a**–**d** similar results were obtained in two replicate experiments.

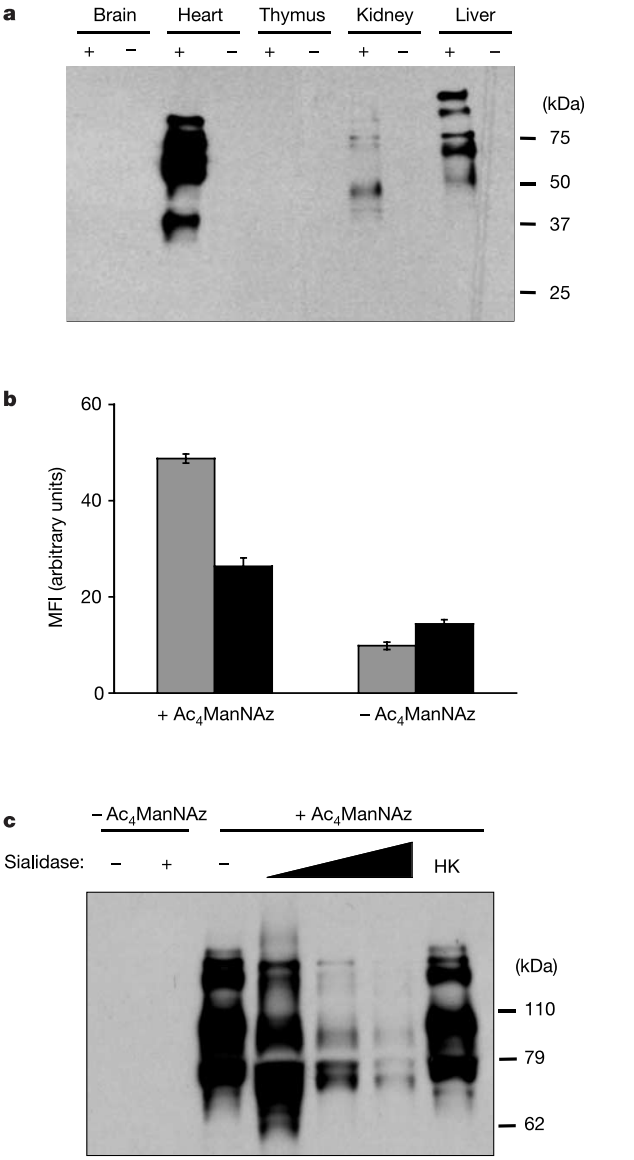


**Figure 3** Analysis of SiaNAz on cells and in tissues. **a**, Western blot analysis of tissue lysates from $Es1^e/Es1^e$ mice administered $Ac_4$ManNAz (+) or vehicle alone (−). The same patterns of labelling were apparent in several experiments. **b**, Splenocytes from B6D2F1 mice treated with $Ac_4$ManNAz or vehicle were treated with *A. ureafaciens* sialidase (black bars) or left untreated (grey bars). The cells were analysed by flow cytometry; error bars represent the standard deviation of the mean for three replicate Staudinger ligation reactions. **c**, Western blot analysis of sialidase-treated (+) or untreated (−) serum samples from mice administered $Ac_4$ManNAz or vehicle. The samples were incubated with active or heat-killed (HK) sialidase. Total protein loading was confirmed by Coomassie-stained protein gel (not shown).

parison to an authentic sample of SiaNAz[23]. Quantification of the total sialic acid population revealed that SiaNAz had replaced approximately 3% of natural sialic acids in this tissue (data not shown). This value is sufficient for detection but unlikely to grossly perturb sialic-acid-dependent interactions. Importantly, no major differences were observed in the sialoglycoprotein profiles of organs from $Ac_4$ManNAz-treated and untreated mice (Supplementary Fig. 1).

Cells coated with SiaNAz *in vivo* are primed for further chemical remodelling within their native physiological environment. To achieve this in practice would require that the Staudinger ligation function on cells within living animals, an unprecedented event for a synthetic reaction. The demands on any reaction in this context are considerable. Aside from displaying extraordinary chemical selectivity, the reactants must possess exquisite biological compatibility; that is, they must not produce harmful side effects nor be prone to rapid metabolic breakdown on the timescale of the reaction. The Staudinger ligation is uniquely poised to fulfil these criteria because its two components, the azide and the phosphine, have been used previously *in vivo*. For example, the azide is a component of the well-known drug AZT (azidothymidine), and phosphine–metal conjugates are established therapeutic and diagnostic agents[24,25].

To test the Staudinger ligation in living animals, we administered $Ac_4$ManNAz (300 mg $kg^{-1}$) intraperitoneally to C57BL/6 mice once daily for 7 days. On the eighth day, mice were injected intraperitoneally with 16 μmol (~1 molar equivalent on the basis of a single dose of 300 mg $kg^{-1}$ $Ac_4$ManNAz) of Phos–Flag. After 90 min, the mice were euthanized, splenocytes were isolated, and cell-surface Flag epitopes were probed by flow cytometry. Only splenocytes from mice treated with both $Ac_4$ManNAz and Phos–Flag displayed a significant increase in fluorescence relative to splenocytes from untreated mice, indicating that the Staudinger ligation had proceeded *in vivo* (Fig. 4, grey bars). We performed similar experiments in which mice were exposed to Phos–Flag for longer time periods before splenocyte analysis. The labelling intensity was significantly reduced after 12 h and no significant labelling was detected after 24 h (data not shown). This time-dependent reduction in labelling might be attributed to degradation of the Flag peptide or to turnover of membrane-associated glycans. No adverse physiological effects were observed even after 24 h of exposure to Phos–Flag, as judged by feeding behaviour and overall activity.

To determine the extent of the *in vivo* Staudinger ligation after 90 min, we subjected harvested splenocytes to further reaction with Phos–Flag *ex vivo* and analysed them by flow cytometry. As shown in Fig. 4 (black bars), cells from mice treated with $Ac_4$ManNAz alone displayed an increase in fluorescence commensurate with the presence of unligated azides. Cells that had been treated with both $Ac_4$ManNAz and Phos–Flag showed a less pronounced increase in fluorescence upon *ex vivo* ligation, suggesting that a significant proportion of the available azides had been ligated *in vivo*. The products of the Staudinger ligation were also observed on serum glycoproteins from mice treated with $Ac_4$ManNAz and Phos–Flag by western blot analysis (Supplementary Fig. 2).

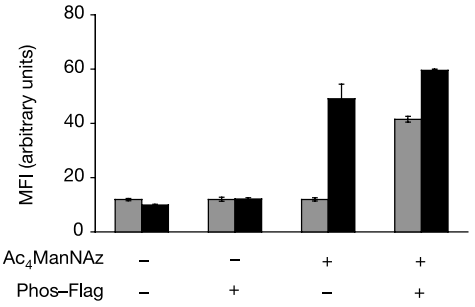


**Figure 4** The Staudinger ligation proceeds *in vivo*. Mice were administered $Ac_4$ManNAz or vehicle once daily for 7 days. On the eighth day, the mice were administered Phos–Flag (16 μmol in ~200 μl PBS) or an equal volume of vehicle. After 1.5 h, splenocytes were treated with FITC–anti-Flag and analysed by flow cytometry (grey bars). A portion of the isolated splenocytes was further reacted with Phos–Flag and analysed as in Fig. 2 (black bars). Error bars represent the standard deviation of the mean for three replicate FITC–anti-Flag labelling reactions or Staudinger ligation reactions.

The ability to chemically modify cell-surface glycans in living animals provides a means to monitor these biopolymers in a physiologically relevant system. For example, the Staudinger ligation might be used to target probes for non-invasive imaging to cells as a function of their glycosylation pattern. Changes in glycosylation associated with stages of organ development or disease progression could be visualized in this fashion. Notably, elevated levels of sialylated glycans have been observed on numerous cancers[15,26,27] and at sites of inflammation[16]. More broadly, the azide can serve as an *in vivo* reporter of secondary metabolite expression. Lipids, steroids and cofactors could potentially be probed if their metabolic enzymes are tolerant of azido precursors.

The range of opportunities provided by the Staudinger ligation underscores the potential impact of bio-orthogonal reactions that can be carried out in whole organisms. An ongoing challenge in the chemistry community is to identify new transformations with the requisite qualities of selectivity and biocompatibility. Indeed, the azide has an alternative mode of reactivity, the 1,3-dipolar cycloaddition with alkynes, which has been used for bioconjugation reactions and could potentially be modified for use *in vivo*[28]. The Staudinger ligation may therefore be the first in a future arsenal of chemical reactions used to probe biology in living animals. □

## Methods

### Compound administration

$Ac_4$ManNAz, ManNAz and Phos–Flag were synthesized according to previously published procedures[7,21]. For metabolic labelling experiments, mice ($Es1^e$/$Es1^e$, B6D2F1 or C57BL/6) were administered daily doses of $Ac_4$ManNAz (0–300 mg $kg^{-1}$ in ~200 μl of 70% aqueous DMSO, from a stock solution of 50 mg $ml^{-1}$) or ManNAz (0–182 mg $kg^{-1}$ in $H_2O$) intraperitoneally for 7 days. Organs were collected 24 h after the final azido-sugar injection. To test the Staudinger ligation in living animals, C57BL/6 mice were administered $Ac_4$ManNAz (300 mg $kg^{-1}$) or vehicle (70% DMSO) intraperitoneally once daily for 7 days. Twenty-four hours after the final $Ac_4$ManNAz bolus, mice were injected intraperitoneally with Phos–Flag (16 μmol in ~200 μl PBS) or vehicle (PBS). Organs were collected 90 min after the Phos–Flag injection.

### Labelling of splenocyte cell-surface azides *ex vivo*

After mice were administered $Ac_4$ManNAz or vehicle alone, their splenocytes were isolated using a standard protocol and probed for the presence of cell-surface azides using a Staudinger ligation assay[9]. Briefly, splenocytes were incubated with 250 μM Phos–Flag for 1 h at room temperature, then treated with FITC–anti-Flag or FITC-conjugated mouse $IgG_1$ isotype control for 30 min on ice and analysed by flow cytometry.

### Lysis of murine organs and western blot analysis

Isolated murine organs were rinsed with PBS (pH 7.4) and homogenized in 2 ml of lysis buffer[29]. To probe for the presence of azides, aliquots of the tissue lysates were diluted 1:1 with 500 μM Phos–Flag and incubated at room temperature for 6–12 h. The samples were analysed by western blot probing with horseradish peroxidase (HRP)–anti-Flag[11].

### Sialidase treatment of splenocytes and organ lysates

Splenocytes from $Ac_4$ManNAz-treated (300 mg $kg^{-1}$ intraperitoneally once daily for 7 days) or untreated B6D2F1 mice were incubated with *Arthrobacter ureafaciens* sialidase (Roche, 20 mU, 100 μl final volume) in sialidase buffer[30]. After 1 h at room temperature, the cells were treated with Phos–Flag followed by FITC–anti-Flag as described above. After a 30 min incubation on ice, the cells were washed and analysed by flow cytometry.

For western blot analysis, murine serum samples were combined with buffer (154 mM NaCl, 50 mM sodium acetate, 9 mM $CaCl_2$, pH 5.5) and *Vibrio cholerae* sialidase (Calbiochem, 0–37 mU, dissolved in the same buffer system) to a total volume of 20 μl. The samples were incubated at 37 °C overnight, then diluted 1:1 with 500 μM Phos–Flag (final Phos–Flag concentration = 250 μM) and incubated at room temperature for 8 h. The samples were further analysed by western blot as described above.

### Splenocyte analysis after *in vivo* Staudinger ligation

Splenocytes from C57BL/6 mice treated with $Ac_4$ManNAz or vehicle (70% DMSO) and Phos–Flag or vehicle (PBS) were isolated and probed for the presence of cell-surface Flag epitopes. Briefly, splenocytes were incubated directly with FITC–anti-Flag (1:900 dilution)

for 30 min on ice. Alternatively, the splenocytes were treated with Phos–Flag *ex vivo* and then FITC–anti-Flag as described above. All cells were analysed by flow cytometry.

Received 12 May; accepted 25 June 2004; doi:10.1038/nature02791.


1. Keppler, O. T., Horstkorte, R., Pawlita, M., Schmidts, C. & Reutter, W. Biochemical engineering of the *N*-acyl side chain of sialic acid: biological implications. *Glycobiology* **11,** 11R–18R (2001).
2. Dube, D. H. & Bertozzi, C. R. Metabolic oligosaccharide engineering as a tool for glycobiology. *Curr. Opin. Chem. Biol.* **7,** 616–625 (2003).
3. Buttner, B. *et al.* Biochemical engineering of cell surface sialic acids stimulates axonal growth. *J. Neurosci.* **22,** 8869–8875 (2002).
4. Keppler, O. T. *et al.* Biosynthetic modulation of sialic acid-dependent virus-receptor interactions of two primate polyoma viruses. *J. Biol. Chem.* **270,** 1308–1314 (1995).
5. Charter, N. W., Mahal, L. K., Koshland, D. E. & Bertozzi, C. R. Differential effects of unnatural sialic acids on the polysialylation of the neural cell adhesion molecule and neuronal behavior. *J. Biol. Chem.* **277,** 9255–9261 (2002).
6. Mahal, L. K., Yarema, K. J. & Bertozzi, C. R. Engineering chemical reactivity on cell surfaces through oligosaccharide biosynthesis. *Science* **276,** 1125–1128 (1997).
7. Saxon, E. & Bertozzi, C. R. Cell surface engineering by a modified Staudinger reaction. *Science* **287,** 2007–2010 (2000).
8. Kayser, H. *et al.* Biosynthesis of a nonphysiological sialic acid in different rat organs, using *N*-propanoyl-D-hexosamines as precursors. *J. Biol. Chem.* **267,** 16934–16938 (1992).
9. Saxon, E. *et al.* Investigating cellular metabolism of synthetic azidosugars with the Staudinger ligation. *J. Am. Chem. Soc.* **124,** 14893–14902 (2002).
10. Hang, H. C., Yu, C., Kato, D. L. & Bertozzi, C. R. A metabolic labeling approach toward proteomic analysis of mucin-type O-linked glycosylation. *Proc. Natl Acad. Sci. USA* **100,** 14846–14851 (2003).
11. Vocadlo, D. J., Hang, H. C., Kim, E. J., Hanover, J. A. & Bertozzi, C. R. A chemical approach for identifying *O*-GlcNAc-modified proteins in cells. *Proc. Natl Acad. Sci. USA* **100,** 9116–9121 (2003).
12. Kohn, M. & Breinbauer, R. The Staudinger ligation—A gift to chemical biology. *Angew. Chem. Int. Edn Engl.* **43,** 3106–3116 (2004).
13. Ovaa, H. *et al.* Chemistry in living cells: Detection of active proteasomes by a two-step labeling strategy. *Angew. Chem. Int. Edn Engl.* **42,** 3626–3629 (2003).
14. Kim, Y. J. & Varki, A. Perspectives on the significance of altered glycosylation of glycoproteins in cancer. *Glycoconj. J.* **14,** 569–576 (1997).
15. Fukuda, M. Possible roles of tumor-associated carbohydrate antigens. *Cancer Res.* **56,** 2237–2244 (1996).
16. Renkonen, J., Tynninen, O., Hayry, P., Paavonen, T. & Renkonen, R. Glycosylation might provide endothelial zip codes for organ-specific leukocyte traffic into inflammatory sites. *Am. J. Pathol.* **161,** 543–550 (2002).
17. Luchansky, S. J. *et al.* Constructing azide-labeled cell surfaces using polysaccharide biosynthetic pathways. *Methods Enzymol.* **362,** 249–272 (2003).
18. Kavarana, M. J., Kovaleva, E. G., Creighton, D. J., Wollman, M. B. & Eiseman, J. L. Mechanism-based competitive inhibitors of glyoxalase I: Intracellular delivery, *in vitro* antitumor activities, and stabilities in human serum and mouse serum. *J. Med. Chem.* **42,** 221–228 (1999).
19. Morton, C. L. *et al.* Activation of CPT-11 in mice: Identification and analysis of a highly effective plasma esterase. *Cancer Res.* **60,** 4206–4210 (2000).
20. Soares, E. R. Identification of a new allele of Es-I segregating in an inbred strain of mice. *Biochem. Genet.* **17,** 577–583 (1979).
21. Kiick, K. L., Saxon, E., Tirrell, D. A. & Bertozzi, C. R. Incorporation of azides into recombinant proteins for chemoselective modification by the Staudinger ligation. *Proc. Natl Acad. Sci. USA* **99,** 19–24 (2002).
22. Stasche, R. *et al.* A bifunctional enzyme catalyzes the first two steps in *N*-acetylneuraminic acid biosynthesis of rat liver—Molecular cloning and functional expression of UDP-*N*-acetyl-glucosamine 2-epimerase/*N*-acetylmannosamine kinase. *J. Biol. Chem.* **272,** 24319–24324 (1997).
23. Luchansky, S. J., Argade, S., Hayes, B. K. & Bertozzi, C. R. Metabolic functionalization of recombinant glycoproteins. *Biochemistry* (in the press).
24. Shaw, C. F. Gold-based therapeutic agents. *Chem. Rev.* **99,** 2589–2600 (1999).
25. Jurisson, S. S. & Lydon, J. D. Potential technetium small molecule radiopharmaceuticals. *Chem. Rev.* **99,** 2205–2218 (1999).
26. Codington, J. F., Klein, G., Silber, C., Linsley, K. B. & Jeanloz, R. W. Variations in the sialic acid compositions in glycoproteins of mouse ascites tumor-cell surfaces. *Biochemistry* **18,** 2145–2149 (1979).
27. Sell, S. Cancer-associated carbohydrates identified by monoclonal antibodies. *Hum. Pathol.* **21,** 1003–1019 (1990).
28. Kolb, H. C. & Sharpless, K. B. The growing impact of click chemistry on drug discovery. *Drug Discov. Today* **8,** 1128–1137 (2003).
29. Martin, D. C., Fowlkes, J. L., Babic, B. & Khokha, R. Insulin-like growth factor II signaling in neoplastic proliferation is blocked by transgenic expression of the metalloproteinase inhibitor TIMP-1. *J. Cell Biol.* **146,** 881–892 (1999).
30. Reichner, J. S., Whiteheart, S. W. & Hart, G. W. Intracellular trafficking of cell surface sialoglycoconjugates. *J. Biol. Chem.* **263,** 16316–16326 (1988).


**Supplementary Information** accompanies the paper on **www.nature.com/nature**.

**Acknowledgements** We thank A. Jamieson, S. Luchansky, H. Hang and P. Drake for discussions. J.A.P. was supported by a HHMI Predoctoral Fellowship and D.H.D. was supported by a National Science Foundation Predoctoral Fellowship. Sialic acid analysis was performed by the UCSD GRTC Glycotechnology Core Resource. This work was supported by grants from Johnson & Johnson (Focused Giving Grant), the Mizutani Foundation for Glycoscience, the US Department of Energy and the National Institutes of Health.

**Competing interests statement** The authors declare that they have no competing financial interests.

**Correspondence** and requests for materials should be addressed to C.R.B. (crb@berkeley.edu).

# Variable ageing and storage of dissolved organic components in the open ocean

**Ai Ning Loh[1]*, James E. Bauer[1] & Ellen R. M. Druffel[2]**

[1]*School of Marine Science, College of William and Mary, PO Box 1346, Gloucester Point, Virginia 23062, USA*
[2]*Department of Earth System Science, University of California at Irvine, 3224 Croul Hall, Irvine, California 92697-3100, USA*

* Present address: Division of Ecological Studies, College of Arts and Sciences, Florida Gulf Coast University, 10501 FGCU Boulevard South, Fort Myers, Florida 33965, USA

**Seawater dissolved organic matter (DOM) is the largest reservoir of exchangeable organic carbon in the ocean, comparable in quantity to atmospheric carbon dioxide[1,2]. The composition, turnover times and fate of all but a few planktonic constituents of this material are, however, largely unknown[3,4]. Models of ocean carbon cycling are thus limited by the need for information on temporal scales of carbon storage in DOM subcomponents, produced via the 'biological pump', relative to their recycling by bacteria[3,4]. Here we show that carbohydrate- and protein-like substances in the open Atlantic and Pacific oceans, though often significantly aged, comprise younger fractions of the DOM, whereas dissolved lipophilic material exhibits up to ~90 per cent fossil character. In contrast to the millennial mean ages of DOM observed throughout the water column, weighted mean turnover times of DOM in the surface ocean are only decadal in magnitude. An observed size–age continuum further demonstrates that small dissolved molecules are the most highly aged forms of organic matter, cycling much more slowly than larger, younger dissolved and particulate precursors, and directly links oceanic organic matter age and size with reactivity[3,5].**

Seawater DOM consists of analytically identifiable biochemicals such as carbohydrates, proteins and lipids, as well as operationally defined and long-lived geomacromolecules (for example, humic and fulvic substances[5,6]). In order to resolve some of the key details of DOM sources and cycling in the oceans, major organic components were extracted from high-molecular-weight ultrafiltered DOM[5] ($DOM_{HMW}$, >1,000 daltons) collected from 1,000–3,000 l of sea water, and analysed for both $\Delta^{14}C$ and $\delta^{13}C$ isotopic signatures. Samples were collected from surface mixed-layer (3–20 m), mesopelagic oxygen-minimum (850–900 m), and abyssal (1,500–1,800 m) depths in the central North Pacific (June 1999) and the Sargasso Sea region of the North Atlantic (June 2000) oligotrophic ocean gyres. The contributions of solvent-extractable lipids, protein-like and carbohydrate-like organic matter (OM), as well as different molecular-weight fractions, to the overall age structure of seawater DOM, were thus established.

By far the most highly aged DOM component was the lipid extract (6.4–17.1 kyr before present, BP; Table 1), with $^{14}C$ ages in the deep Pacific representing the greatest yet observed for any component of seawater OM. The lipid extract was considerably older by ~5–13 kyr than the total $DOM_{HMW}$ and unfractionated, bulk DOM (ΣDOM) pools (Tables 1 and 2; Fig. 1a). Furthermore, at all mesopelagic and abyssal depths, the lipid extract and $DOM_{HMW}$ were older in the Pacific than in the Atlantic, similar to the ocean–ocean offsets observed for ΣDOM[6,7] (Table 1) and presumably due to cumulative ageing during deep water-mass transit[8]. Conversely, mixed-layer lipid extract, $DOM_{HMW}$ and ΣDOM were all older in the Atlantic than in the Pacific (Tables 1 and 2), suggesting possible aged North American continental or atmospheric inputs there[9]. The highly $\delta^{13}C$-depleted signatures of lipid extracts (Table 1, Fig. 1b) are consistent with isotopic fractionations during cellular lipid